Sensitive detection of entanglement in exciton-polariton condensates via spin squeezing

Jingyan Feng,[1] Ebubechukwu O. Ilo-Okeke,[2,3] Alexey N. Pyrkov,[4] Alexis Askitopoulos,[5] and Tim Byrnes[1,2,6,7,8,*]

[1]*State Key Laboratory of Precision Spectroscopy, School of Physical and Material Sciences, East China Normal University, Shanghai 200062, China*

[2]*New York University Shanghai, 1555 Century Ave., Pudong, Shanghai 200122, China*

[3]*Department of Physics, School of Physical Sciences, Federal University of Technology, P. M. B. 1526, 0werri 460001, Nigeria*

[4]*Institute of Problems of Chemical Physics of Russian Academy of Sciences, Acad. Semenov av. 1, Chernogolovka, Moscow Region 142432, Russia*

[5]*Skolkovo Institute of Science and Technology, Bolshoy Boulevard 30, bld. 1, Moscow 121205, Russia*

[6]*NYU-ECNU Institute of Physics at NYU Shanghai, 3663 Zhongshan Road North, Shanghai 200062, China*

[7]*National Institute of Informatics, 2-1-2 Hitotsubashi, Chiyoda-ku, Tokyo 101-8430, Japan*

[8]*Department of Physics, New York University, New York, NY 10003, USA*

(Received 2 December 2020; revised 11 May 2021; accepted 6 July 2021; published 30 July 2021)

We propose a method of generating and detecting entanglement via spin squeezing in an exciton-polariton condensate. Spin squeezing is a sensitive detector of entanglement because any squeezing below shot noise implies entanglement. In our scheme, two polariton spin species are resonantly pumped, forming a particle number fluctuating effective spin. The naturally occurring nonlinear interactions between the polaritons produce an effective one-axis squeezing interaction, which drives the system toward a spin-squeezed state at steady-state. We investigate the squeezing level that is attainable at the steady state for realistic experimental parameters and show the favorable parameters for strong squeezing. The amount of squeezing tends to improve with larger pumping, due to the bosonic enhancement of the one-axis twisting Hamiltonian. Using number-fluctuating versions of the Wineland squeezing criterion and optimal spin inequalities, we show how multipartite entanglement can be detected.

DOI: 10.1103/PhysRevA.104.013318

I. INTRODUCTION

Entanglement is considered one of the hallmarks of quantum mechanics, which distinguishes it from classical physics [1–5]. While it is most commonly associated with the microscopic world, for sufficiently coherent systems and using states that are relatively robust under decoherence, it has been observed also at the larger scale [6–9]. Entanglement in the mesoscopic regime has been achieved in experiments with superconductors, resulting in the recent fast progress of superconducting quantum computers [10–13]. Entanglement plays a central role in quantum technologies to obtain practical advantages over devices based on classical physics. This has made the generation of entanglement one of the central tasks that must be achieved for any experimental platform in quantum information science.

In the context of quantum metrology, squeezed states are a specific type of entangled state that allows for enhanced measurements beyond the standard quantum limit [14–16]. While squeezing was first studied in the context of optics, analogous states have been studied for many-particle systems such as atomic ensembles and Bose-Einstein condensates (BECs) [17]. Numerous studies have aimed at realizing quantum correlations and entanglement within an atomic BEC and spin squeezing is one of the most well-studied directions [18–22]. More recently, the generation of many-particle entanglement within a single atomic BEC has also been investigated and realized in some experiments; in this case, entanglement was detected between different spatial regions of a single BEC [23–25]. This has spurred the study of more specific types of entanglement, such as Einstein-Podolsky-Rosen (EPR) steering and Bell correlations [26]. Currently, there has not been an experimental demonstration of entanglement between spatially separated BECs but there have been numerous theoretical proposals using a variety of methods based on interactions [27–29], Rydberg excitations [30], or light-mediated methods [31–35]. In addition to quantum metrology applications, entanglement between atomic ensembles has been proposed to be useful for quantum information applications such as quantum communications and computation [18,19,36–39].

Another rich platform exhibiting quantum degeneracy is that of exciton-polariton condensates [40–48]. Exciton-polaritons are a superposition of an exciton (an electron-hole bound pair) and a cavity photon formed in planar semiconductor microcavity structures. The extremely light effective mass of the exciton-polaritons, inherited from the cavity photons, led to the milestone achievement of BECs [40,49,50]. Meanwhile, the matter component produces an effective nonlinear interaction which originates from a Coulomb exchange [51–53]. This combination makes them fascinating hybrid

*tim.byrnes@nyu.edu

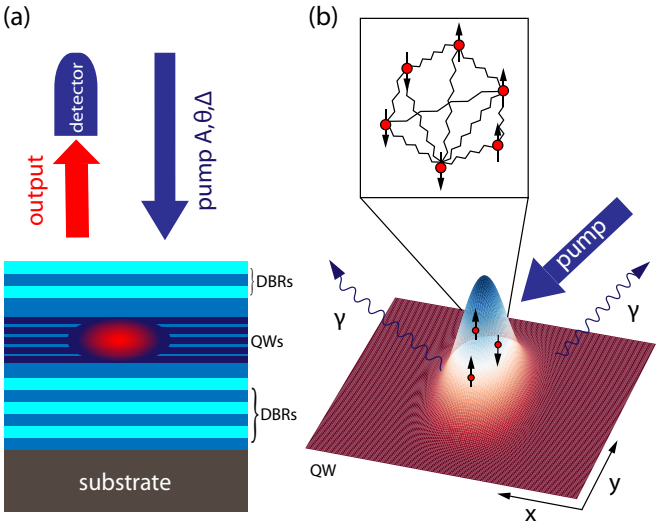

FIG. 1. Schematic experimental system that we consider in this paper. (a) A semiconductor microcavity formed by quantum wells (QWs) sandwiched by distributed Bragg reflectors (DBR) is pumped using laser light to excite the exciton-polaritons. The condensate is represented by the circle in QWs. At sufficient densities the exciton-polaritons form a condensate. Polaritons leak through the mirrors to produce photoluminescence, which is imaged using a camera. (b) The condensate is formed by exciton-polaritons of spin ± 1 species, which have a natural non-linear interaction. As the system is pumped, the many-particle system approaches steady-state involving entanglement (zig-zag lines). By detecting the polarization of the photoluminescence, entanglement can be inferred from the presence of spin squeezing.

systems for studying highly coherent phenomena familiar from optical systems, while simultaneously having matterlike properties [54–61]. They also have the advantage that, using different semiconductor materials, it is possible to achieve higher condensation temperatures, even at room temperature [62–66]. Experimental investigations of squeezing in polaritons has been shown in several works using four-wave mixing and resonant excitation techniques [67–69]. It is only recently that beyond mean-field effects have been experimentally detectable in polariton condensates [70]. However, to date, there has not been any explicit demonstration of entanglement in polariton condensates, either within a single condensate or between two spatially separate condensates.

In this paper, we examine an approach to generate entanglement within an exciton-polariton condensate. The origin of the entanglement is the nonlinear self-interactions between exciton-polaritons. In our proposed setup, the two spin species of exciton-polaritons are pumped initially with linearly polarized light (Fig. 1). This induces a macroscopic population of exciton-polaritons within the QW, containing a superposition of the two spin species. Due to the exchange interaction between excitons of the same spin, this produces an effective one-axis twisting type of interaction, when written in the total spin language. By examining the spin variance and driving the system toward the steady state, we show that this forms a spin-squeezed state. Then, using well-developed relations between spin squeezing and entanglement, we deduce the presence of entanglement in the coherent ensemble of exciton-polaritons.

Entanglement detection via spin squeezing provides a sensitive way of inferring entanglement in the system. It is well-established that any spin squeezing that is below shot noise (i.e., 0 dB) implies the presence of entanglement [18]. This is in contrast to quadrature squeezing, where at least 3 dB of squeezing is required to detect entanglement [71]. We note that a similar approach of observing polarization squeezing and entanglement has been demonstrated with cold atoms [72,73]. In the work of Josse *et al.*, the atomic excitation is created by linearly polarized light passing through cold cesium atoms. For polaritons considered here, the squeezing is as a result of the exchange interactions among the electron-hole pairs, giving rise to self-interactions among polaritons of the same species. Polarization squeezed light and the squeezed exciton-polariton condensates have no fixed total particle number, hence it is important to take into effect the of number fluctuations. We discuss appropriate criteria that allows for detection of entanglement in such highly number-fluctuating states.

This paper is organized as follows. In Sec. II, we introduce the theoretical model for the pumped spinor exciton-polariton condensate. In Sec. IV, we discuss and analyze our simulation results by calculating quantities such as the average particle number, spin Q functions, and variances. In Sec. V, we translate what this means in terms of entanglement using different detection schemes. Finally, in Sec. VI, we summarize and discuss our results.

II. THEORY OF SPIN SQUEEZING WITH PUMPED POLARITONS

A. Master equation

We consider a system of exciton-polaritons within a semiconductor microcavity as shown in Fig. 1(a). Excitons within a high-mobility quantum well (QW) are strongly coupled to cavity photons defined by a distributed Bragg reflector (DBR). Two polariton spin species $s = \pm 1$ exist in the microcavity, which can be distinguished by the polarization of the light that emerges as photoluminescence from the cavity. The polaritons are resonantly pumped using an external laser light of linearly polarized light with a rate A, which populates the two spin species. The orientation of the linearly polarized light changes the relative phase of the polariton spin species. The microcavity has a loss rate of γ for each of the spin species. Polaritons of the same species interact with energy $\hbar U$, and have a cross-spin interaction of energy $\hbar V$.

Such a system can be described by the master equation in the interacting picture as

$$\frac{d\rho}{dt} = -\frac{i}{\hbar}[H_0 + H_{\text{pump}} + H_{\text{int}}, \rho] - \frac{\gamma}{2}\mathcal{L}[a, \rho] - \frac{\gamma}{2}\mathcal{L}[b, \rho], \tag{1}$$

where the Hamiltonians are defined,

$$H_0 = \hbar\Delta(a^\dagger a + b^\dagger b),$$
$$H_{\text{pump}} = \hbar A(a^\dagger e^{-i\theta_a} + a e^{i\theta_a} + b^\dagger e^{-i\theta_b} + b e^{i\theta_b}),$$

$$H_{\rm int} = \frac{\hbar U}{2}(a^\dagger a(a^\dagger a - 1)) + \frac{\hbar U}{2}(b^\dagger b(b^\dagger b - 1)) + \hbar V a^\dagger a b^\dagger b, \tag{2}$$

where $a^\dagger, b^\dagger$ and a, b are the creation and annihilation operators for the two zero-momentum polariton spin species $s = \pm 1$, respectively, which obey bosonic commutation relations

$$[a, a^\dagger] = [b, b^\dagger] = 1, \quad [a, b] = 0. \tag{3}$$

We neglect higher momentum polariton modes since these do not contribute to the spin squeezing entanglement that we are interested in for this study. Here, the Hamiltonian H_0 defines the energy $\hbar\Delta$ of the zero-momentum polaritons relative to the pump laser. $H_{\rm pump}$ is the Hamiltonian for the pump laser with amplitude A, and θ_a and θ_b are the pumping phases of the laser for modes a and b respectively. The Hamiltonian $H_{\rm int}$ contains the nonlinear interaction with energy $\hbar U$ between the same spins and $\hbar V$ for different spins. The superoperator

$$\mathcal{L}[a, \rho] = a^\dagger a\rho + \rho a^\dagger a - 2a\rho a^\dagger, \quad \mathcal{L}[b, \rho] = b^\dagger b\rho + \rho b^\dagger b - 2b\rho b^\dagger \tag{4}$$

is the Lindbladian loss for photons leaking through the cavity. Polaritons are lost with a rate γ.

The nonlinear terms in the Hamiltonian $H_{\rm int}$ are expected to produce spin squeezing since the self-interaction terms can be rewritten as

$$H_{\rm int} = \frac{(U - V)}{4}(S_z)^2 + \frac{(U + V)}{4}\mathcal{N}^2 - \frac{U\mathcal{N}}{2}, \tag{5}$$

where we defined the total number operator

$$\mathcal{N} = a^\dagger a + b^\dagger b, \tag{6}$$

and the Schwinger boson (total spin) operators as

$$S_x = a^\dagger b + b^\dagger a, \quad S_y = i(b^\dagger a - a^\dagger b), \quad S_z = a^\dagger a - b^\dagger b, \tag{7}$$

which obey the commutation relations

$$[S_l, S_m] = 2i\epsilon_{lmn}S_n, \tag{8}$$

where ϵ_{lmn} is the Levi-Civita symbol and $l, m, n \in \{x, y, z\}$. The total number operator commutes with all spin operators

$$[\mathcal{N}, S_l] = 0, \tag{9}$$

hence they share the same set of eigenstates. In the interaction Hamiltonian (5), the $(S_z)^2$ term is known to produce a one-axis twisting squeezing interaction [14]. Note that if $U = V$, then the $(S_z)^2$ term cancels and there will not be any squeezing.

B. Spin mapping

A major difference between atom BECs and exciton-polariton condensates is that the latter is an open dissipative system and does not obey a conservation law for the total polariton number. In an atomic system, the atom number can be considered to be constant shot to shot, but in the polariton system the pumping terms $H_{\rm pump}$ in (1) actively produce superpositions in the polariton number states. Ultimately, we will be interested in generating spin squeezing between modes a and b, and thereby generating entanglement. In this section, we discuss how a system without a fixed particle number can be mapped into an effective spin space.

To identify the spin mapping, first let us expand the density matrix as

$$\rho = \sum_{klk'l'} \rho_{klk'l'} |k, l\rangle\langle k', l'|, \tag{10}$$

where

$$|k, l\rangle = \frac{(a^\dagger)^k (b^\dagger)^l}{\sqrt{k!l!}}|0\rangle \tag{11}$$

are the normalized Fock states. For atomic BECs, the number of atoms can often be considered to be fixed, meaning that k and l satisfy the relation $k + l = N$, where N is the fixed atom number. To identify the different spin sectors, we project the density matrix of the full Hilbert space to its equivalent spin version with a total of N particles. We define the density matrix in the N-particle sector as

$$\rho_N = \frac{\Pi_N \rho \Pi_N}{p_N}, \tag{12}$$

where

$$\Pi_N = \sum_{k=0}^{N} |k, N - k\rangle\langle k, N - k| \tag{13}$$

is the projector on the N-particle subspace. The denominator in (12) is needed such as to normalize the state properly. The probability of projection on the N-particle sector is defined as

$$p_N = {\rm Tr}(\Pi_N \rho \Pi_N). \tag{14}$$

As usual, p_N is a probability distribution and satisfies

$$\sum_N p_N = 1. \tag{15}$$

We introduce the notation that any expectation value with the subscript N should be taken with respect to the state ρ_N,

$$\langle \mathcal{X} \rangle_N \equiv {\rm Tr}(\rho_N \mathcal{X}), \tag{16}$$

for any operator $\mathcal{X}$. Any state after projection is in a fixed total polariton number subspace

$$\langle \mathcal{N} \rangle_N = {\rm Tr}(\mathcal{N}\rho_N) = N. \tag{17}$$

The number projected state can be used to form the number averaged density matrix:

$$\rho_\Pi = \sum_N \Pi_N \rho \Pi_N = \sum_N p_N \rho_N. \tag{18}$$

This is a mixture of spin density matrices of different particle numbers. While $\rho_\Pi \neq \rho$ in general, for expectation values of any product of spin operators it is possible to use either state. For example, for a single spin operator

$$\langle S_l \rangle_{\rho_\Pi} = {\rm Tr}(S_l \rho_\Pi) = \sum_N p_N {\rm Tr}(S_l \rho_N)$$

$$= \mathrm{Tr}\left(\sum_N \Pi_N S_l \Pi_N \rho\right)$$
$$= \mathrm{Tr}(S_l \rho)$$
$$= \langle S_l \rangle_\rho, \tag{19}$$

where we used the fact that $[S_l, \Pi_N] = 0$, $\Pi_N^2 = \Pi_N$, and $\sum_N \Pi_N = I$, and the cyclic property of the trace $\mathrm{Tr}(XYZ) = \mathrm{Tr}(ZXY)$. For any product of spin and number operators, the same logic holds, as the particle number is conserved. Thus, in terms of evaluating expectation values of spin operators, one does not need to use the number projected state ρ_Π, since the spin operators (7) do not mix different number sectors.

C. Noninteracting limit

We illustrate the spin mapping procedure by a simple but relevant example. Consider the limiting case of the master equation (1) where interactions are set to zero $U = V = 0$. In this case, the master equation can be exactly solved, and the steady-state solutions take the form of a coherent state. To find the steady-state amplitudes, we multiply (1) by a and b, respectively, to obtain

$$\frac{d\langle a\rangle}{dt} = -i(\Delta\langle a\rangle + Ae^{-i\theta_a}) - \frac{\gamma\langle a\rangle}{2},$$
$$\frac{d\langle b\rangle}{dt} = -i(\Delta\langle b\rangle + Ae^{-i\theta_b}) - \frac{\gamma\langle b\rangle}{2}. \tag{20}$$

Setting the time derivatives to zero, we obtain the steady-state coherent state amplitudes

$$\alpha_0 = \frac{Ae^{-i(\theta_a+\pi/2)}}{\gamma/2 + i\Delta},$$
$$\beta_0 = \frac{Ae^{-i(\theta_b+\pi/2)}}{\gamma/2 + i\Delta} \tag{21}$$

for modes a and b, respectively. The steady-state final state is thus

$$|\alpha_0\rangle|\beta_0\rangle = e^{-(|\alpha_0|^2+|\beta_0|^2)/2} e^{\alpha_0 a^\dagger} e^{\beta_0 b^\dagger}|0\rangle. \tag{22}$$

Now let us use the spin mapping to find the effective spin state in the N-particle sector. Applying the projector (13), we have

$$\Pi_N|\alpha\rangle|\beta\rangle = e^{-(|\alpha_0|^2+|\beta_0|^2)/2}\Pi_N \sum_{kl} \frac{\alpha_0^k \beta_0^l}{\sqrt{k!l!}}|k, l\rangle$$
$$= e^{-(|\alpha_0|^2+|\beta_0|^2)/2} \sum_k \frac{\alpha_0^k \beta_0^{N-k}}{\sqrt{k!(N-k)!}}|k, N-k\rangle$$
$$= \sqrt{p_N}\left|\frac{\alpha_0}{\sqrt{|\alpha_0|^2+|\beta_0|^2}}, \frac{\beta_0}{\sqrt{|\alpha_0|^2+|\beta_0|^2}}\right\rangle\!\!\rangle. \tag{23}$$

Here we defined the spin coherent state

$$|\alpha, \beta\rangle\rangle = \frac{1}{\sqrt{N!}}(\alpha a^\dagger + \beta b^\dagger)^N|0\rangle$$
$$= \sum_k \sqrt{\binom{N}{k}}\alpha^k \beta^{N-k}|k, N-k\rangle, \tag{24}$$

which has a fixed particle number $\mathcal{N}|\alpha, \beta\rangle\rangle = N|\alpha, \beta\rangle\rangle$ and is normalized for $|\alpha|^2 + |\beta|^2 = 1$. The probability of obtaining this particle number sector is

$$p_N = e^{-(|\alpha_0|^2+|\beta_0|^2)}\frac{(|\alpha_0|^2+|\beta_0|^2)^N}{N!}. \tag{25}$$

The above result (23) shows that, as expected, no squeezing or entanglement is present when there are no interactions, since a spin coherent state is an example of a state that is at the standard quantum limit [17].

The number averaged density matrix is then

$$\rho_\Pi = \sum_N p_N \left|\frac{\alpha_0}{\sqrt{|\alpha_0|^2+|\beta_0|^2}}, \frac{\beta_0}{\sqrt{|\alpha_0|^2+|\beta_0|^2}}\right\rangle\!\!\rangle$$
$$\times \left\langle\!\!\left\langle \frac{\alpha_0}{\sqrt{|\alpha_0|^2+|\beta_0|^2}}, \frac{\beta_0}{\sqrt{|\alpha_0|^2+|\beta_0|^2}}\right|. \tag{26}$$

This is an incoherent mixture of spin coherent states with the same Bloch sphere coordinates.

D. Observables

Here we define the main observables that are relevant for showing spin squeezing in the polariton system.

1. Variances

The most direct way to show spin squeezing is by evaluating the variance of the spin operators (7). The variance is evaluated along the perpendicular direction to the average spin. For example, if the average spin is in the S_x direction, then the variance is evaluated in the S_y-S_z plane

$$S_\Phi = S_y \sin\Phi + S_z \cos\Phi, \tag{27}$$

where Φ is the angle with respect to the z axis. The variance for the N-particle sector is then calculated as

$$\mathrm{Var}_N(S_\Phi) = \langle S_\Phi^2\rangle_N - \langle S_\Phi\rangle_N^2, \tag{28}$$

where the subscript N on the variance indicates that the fixed number state ρ_N is used. The spin in the particle number sector N is said to be squeezed if [14,17,74]

$$\mathrm{Var}_N(S_\Phi) < N. \tag{29}$$

For example, for a spin coherent state $|1/\sqrt{2}, 1/\sqrt{2}\rangle\rangle$, the variance obeys $\mathrm{Var}_N(S_\Phi) = N$, and hence is unsqueezed.

Since each particle sector N has a different threshold for squeezing as seen in (29), we define a normalized variance $\mathrm{Var}_N(S_\Phi)/N$ such that the squeezing threshold is 1. Then the average squeezing parameter across particle number sectors labeled by N can be defined as

$$\chi(\Phi) = \sum_N p_N\left(\frac{\mathrm{Var}_N(S_\Phi)}{N}\right). \tag{30}$$

In the zero-particle sector, we define the state to have no squeezing such that the term in the brackets for $N = 0$ is set to 1. A state exhibits squeezing on average if

$$\chi(\Phi) < 1. \tag{31}$$

2. Spin Q distribution

To visualize the quantum state in the N-particle sector, an effective way is to find the spin Q distribution, which we define as [75]

$$Q_N(\theta,\phi) = \frac{(N+1)}{4\pi}\left\langle\left\langle \cos\frac{\theta}{2}, e^{i\phi}\sin\frac{\theta}{2}\right|\rho_N \times \left|\cos\frac{\theta}{2}, e^{i\phi}\sin\frac{\theta}{2}\right\rangle\right\rangle, \tag{32}$$

where the spin coherent states are defined in (24) and are taken to be in the N-particle sector. Each of the Q_N functions are normalized,

$$\int Q_N(\theta,\phi)\sin\theta d\theta d\phi = 1, \tag{33}$$

hence we may then take the average and calculate its average Q function across all the particle number sectors. We hence define

$$Q(\theta,\phi) = \sum_N p_N Q_N(\theta,\phi). \tag{34}$$

This is also a normalized function:

$$\int Q(\theta,\phi)\sin\theta d\theta d\phi = 1. \tag{35}$$

III. SIMULATING THE MASTER EQUATION

A. Parameters

We first discuss the parameters of the evolution of the central equation (1) that we calculate in this study. Dividing (1) by γ throughout, we have a total of six independent parameters: the detuning Δ/γ, pump rate A/γ, the pump phases θ_a, θ_b, intraspecies interaction U/γ, interspecies interaction V/γ. We assume that the first four of these parameters can be freely changed (within reasonable physical ranges) by simply adjusting the laser parameters. For example, by adjusting the frequency of the pump laser around the lower polariton resonance, Δ/γ can be adjusted, while the intensity, phase, and polarization of the laser affects $A/\gamma, \theta_a, \theta_b$. While γ itself is not tunable since it is set by the physical characteristics of the microcavity, the ratio of four of the parameters is adjustable.

Meanwhile, the polariton-polariton interactions are less easily adjusted and are typically given by naturally occurring parameters. The intraspecies interaction can be estimated from

$$U = \frac{30e^2 a_B |X|^4}{\hbar\pi^3\epsilon\mathcal{A}}, \tag{36}$$

where e is the electronic charge, X is the exciton Hopfield coefficient, ϵ is the effective permittivity in the semiconductor, a_B is the Bohr radius, and $\mathcal{A}$ is the trapping area [51,53,54,76]. In GaAs-based structures with $a_B = 10$ nm, permittivity $\epsilon = 13\epsilon_0$, zero detuning $X = 1/\sqrt{2}$, and a spot size of 1 μm, we have $\hbar U \sim 4$ μeV. Using a conservative estimate of the polariton lifetime using low-Q cavities where $1/\gamma \sim 6$ ps, we obtain $U/\gamma \sim 0.05$. For a higher-Q cavity where $1/\gamma \sim 36$ ps, we have $U/\gamma \sim 0.3$. As explained in Refs. [51,53,54], the repulsive interaction between low-momentum polaritons originate from exchange interaction between electrons and holes that compose the excitons. Thus, for different spin species, there is no repulsive interaction to lowest order. We thus set the interspin interactions to $V = 0$ throughout [51,77]. We note that tuning the interactions in exciton-polariton condensates has been achieved in Refs. [78–81].

B. Numerical methods

QuTip [82,83] was used to perform the time evolution of the master equation (1). In any numerical simulation, truncation of the Hilbert space is required, since the polaritons occupy an infinite dimensional space. We employ a simple strategy of truncating the Fock states (11) such that the maximum range is $k, l \in [0, N_{\max}]$. What this means in terms of the evolution of (1) is that any state that is connected where $k, l > N_{\max}$ is set to zero. This allows us to obtain a truncated version of (1) within the Fock states with $k, l \in [0, N_{\max}]$. This means that all quantities involving a summation over Fock states such as (10), (15), and (34) have their upper limits changed to $N_{\max}$.

Since we will later perform a spin mapping by applying the projection operator (13), we discuss the effect of the truncation on the relevant spin spaces. Consider a plot of the possible Fock states (11) on a square lattice such that the horizontal axis labels the $k \geqslant 0$ and the vertical labels the $l \geqslant 0$. Then the effect of the truncation is to keep states within a square region $0 \leqslant k, l \leqslant N_{\max}$. Lines of constant N, as projected upon by (13), are along the negative diagonal lines such that $l = N - k$. What this amounts to is that for a given $N_{\max}$, the largest N that can be calculated without truncation is $N = N_{\max}$. One may ask why the region with $l > N - k$ is still kept in the context of calculating the effective spin. First, to calculate observables for a given spin sector N, generally one requires taking $N_{\max} > N$ such that truncation effects do not affect the calculation. Second, we will primarily be dealing with states with spins in the vicinity of the equator of the Bloch sphere since in (1), a, b are pumped with the same amplitude A. What this results in is that the populations of a, b are always of a similar order, such that $l \sim k$. Thus, in terms of our truncation, the most important regions are along the positive diagonal $l \sim k$, and along the edges of the truncated square the population is smaller. Thus as long as $N_{\max}$ is large enough to keep track of the primarily populated states, the simple truncation approach is an effective method to keep the most relevant states.

IV. STEADY-STATE SOLUTIONS OF THE MASTER EQUATION

We now discuss the numerical results obtained by directly simulating the master equation (1). We first discuss how the steady-state solutions are obtained, then directly calculate the Q functions in various particle sectors, as well as the average values. Then the amount of squeezing is evaluated using variances and the squeezing parameter χ.

A. Reaching steady-state and numerical truncation

To obtain the steady-state solutions, we numerically evolve (1) until static solutions are reached. To evaluate whether the steady state has been reached, we calculate the expectation

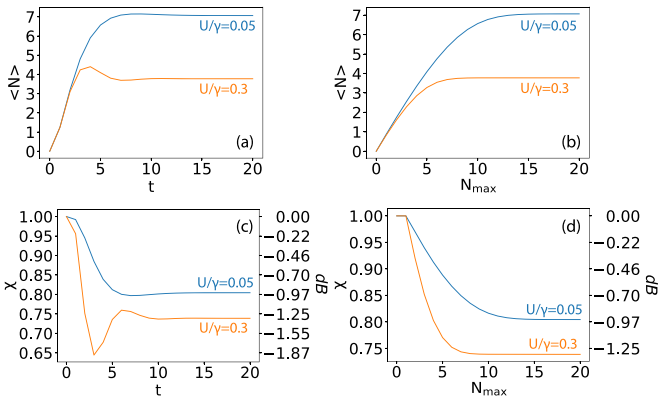

FIG. 2. Average particle number (6) and variance (30) versus evolution time t (a), (c) and $N_{\max}$ (b), (d), respectively. Common parameters are $\Delta/\gamma = 0, A/\gamma = 1, V = \theta_a = \theta_b = 0$.

value of the total number operator $\mathcal{N}$. The results are shown in Fig. 2. We expect that the timescale of the approach to the steady state is set by the polariton loss rate γ, hence the steady state should be achieved for several multiples of the dimensionless unit γt. We find that after approximately $\gamma t = 10$, the average number remains constant for all cases.

The steady-state particle number is generally a function of all parameters of the master equation (1). From (21), we obtain that the steady-state total particle number in the noninteracting limit is

$$\langle \mathcal{N} \rangle \approx |\alpha_0|^2 + |\beta_0|^2 = \frac{2A^2}{\gamma^2/4 + \Delta^2}. \tag{37}$$

For the parameters used in Fig. 2, the steady-state values should approach $\langle \mathcal{N} \rangle = 8$. The steady-state particle number is generally seen to decrease with the interaction strength U for the same pumping rate A, where for the $U/\gamma = 0.05$ case a similar value to the noninteracting case is achieved, but for $U/\gamma = 0.3$ the average number is significantly reduced. We attribute this to the interactions giving an effective detuning effect such that the pumping is less efficient at generating polaritons at the target frequency as the polariton population increases.

In Fig. 2(b), we examine the effect of the truncation on the average polariton number on the steady-state values. The average polariton numbers are calculated at $\gamma t = 20$, which well approximates the steady-state results. We see that convergence is generally attained when $N_{\max} \sim \langle \mathcal{N} \rangle$ as expected, since the calculation is large enough to contain the dominant polariton population. For larger pump rates, as expected, a larger $N_{\max}$ is required to reach convergence. Convergence shows that by taking $N_{\max}$ large enough, the effect of the numerical truncation can be made to not affect the physical results.

To verify that the attainment of the steady state and the dependence on the truncation is well estimated using the number operator, we also calculate the time and $N_{\max}$ dependence for the squeezing parameter (30). We generally see similar results, where the steady state is attained for $\gamma t = 10$ and convergence with $N_{\max} \sim \langle \mathcal{N} \rangle$, at similar values as calculated with the average particle number. We will henceforth consider all our results after they have reached the steady state, and take $N_{\max}$ large enough such that the physical results are independent of the truncation.

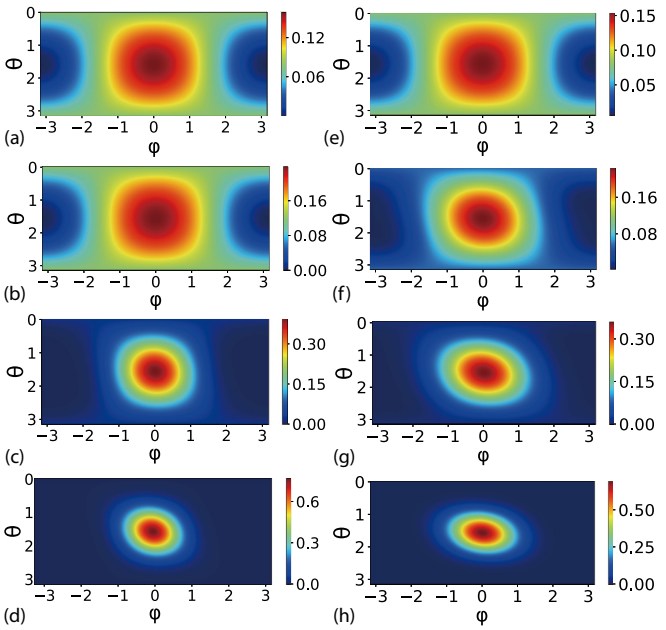

FIG. 3. Individual Q_N-function (32) for a fixed polariton number N in the (θ, ϕ) plane. Parameters are $U/\gamma = 0.05$ for (a) $N = 1$, (b) $N = 2$, (c) $N = 4$, (d) $N = 9$, and $U/\gamma = 0.3$ for (e) $N = 1$, (f) $N = 2$, (g) $N = 4$, (h) $N = 9$. Common parameters are $\Delta/\gamma = 0, A/\gamma = 1$ and $V = \theta_a = \theta_b = 0, N_{\max} = 20$. Angles are in units of radians.

B. Q functions and variances

We now turn to calculating the Q_N functions as defined in (32) for various particle sectors. The results are shown in Fig. 3. We choose parameters such that the polaritons are pumped with $\theta_a = \theta_b = 0$ and $\Delta = 0$, which in the noninteracting limit generates coherent states with $\alpha = \beta = 2A/\gamma$ according to (21). After the spin mapping, this corresponds to a spin coherent state $|1/\sqrt{2}, 1/\sqrt{2}\rangle$ which is polarized in the S_x direction from (23). The first thing we notice is that the size of the Q_N functions decrease with N. This is as expected since the size of the Q_N functions scale as $\sim 1/\sqrt{N}$ [17].

More importantly, we see that the Q_N functions show more squeezing for the larger particle number sector N. For instance, the squeezing is higher at $N = 9$ compared to the case $N = 4$ in Figs. 3(c) and 3(d) and Figs. 3(g) and 3(h). Unsqueezed Q_N functions appear as a symmetric Gaussian-shaped distribution, and it is clear that squeezing is being generated for the larger N values. We attribute this to the fact that for larger systems the same amount of squeezing is attained for shorter interaction times. The optimal squeezing time scales as $\sim 1/N^{2/3}$ [14,17], which originates from the bosonic enhancement of the squeezing interaction Hamiltonian S_z^2. Thus, for the larger particle number sectors, the interaction only needs to act for a smaller time to achieve the same effect. We can imagine this physically that the polaritons enter the cavity for a typical time $1/\gamma$, and within this time they become squeezed. For the larger particle-number sectors,

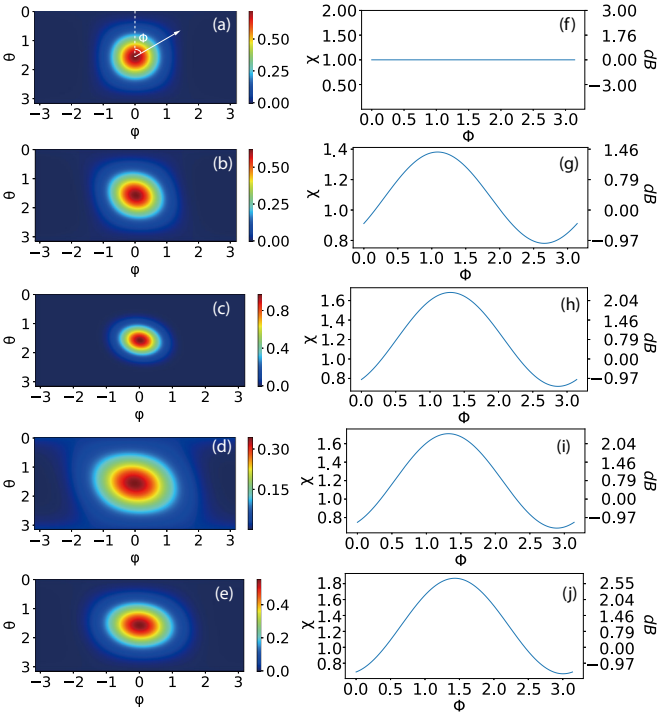

FIG. 4. Average Q function (34) in the (θ, ϕ) plane and variance (30) as a function of Φ for (a) and (f) $A/\gamma = 1, U/\gamma = 0$; (b) and (g) $A/\gamma = 1, U/\gamma = 0.05$; (c) and (h) $A/\gamma = 2, U/\gamma = 0.05$; (d) and (i) $A/\gamma = 1, U/\gamma = 0.3$; (e) and (j) $A/\gamma = 2, U/\gamma = 0.3$. Common parameters are $\Delta/\gamma = 0$ and $V = \theta_a = \theta_b = 0$, $N_{\max} = 20$. Angles are in units of radians.

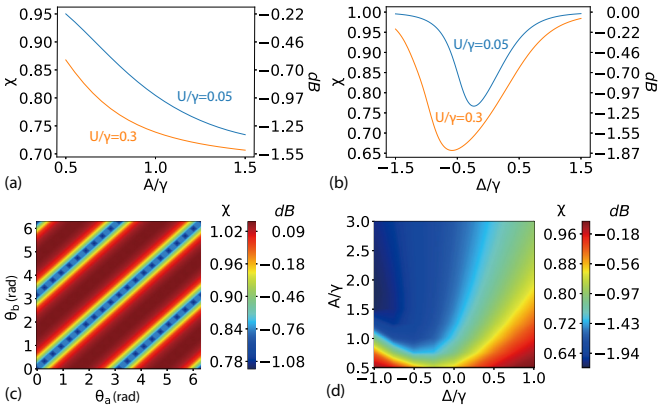

FIG. 5. Optimal spin squeezing χ of polaritons at steady state. In each case, the optimal spin direction Φ in (30) is found as a function of (a) A/γ with $\Delta/\gamma = \theta_a = \theta_b = 0$; (b) Δ/γ with $A/\gamma = 1, \theta_a = \theta_b = 0$; (c) θ_a, θ_b with $\Delta/\gamma = -0.25, A/\gamma = 1, U/\gamma = 0.05, \theta_a = \theta_b = 0$; (d) $A/\gamma, \Delta/\gamma$ with $U/\gamma = 0.3, \theta_a = \theta_b = 0$. Common parameters are $V = 0$, $N_{\max} = 20$.

the squeezing timescales are shorter by $\sim 1/N^{2/3}$, hence there is a larger squeezing effect.

The results as shown in Fig. 3 experimentally would correspond to performing a measurement on various particle-number sectors N and plotting the Q function for these postselected results. Since N varies from shot to shot, to measure the full Q function one would need to take a large number of measurements for each θ and ϕ to have a chance of getting shots with the same particle number N to compose the images. To remove the postselection on N, we hence also look at the average Q function (34) which is over all particle number sectors. The results for various choices of parameters are shown in Figs. 4(a)–4(e). We observe that for all parameter choices with $U > 0$, there is a squeezing effect, where there is a deviation from the circular distribution obtained for $U = 0$. The squeezing in the diagonal direction is as expected for a one-axis squeezing interaction, where the optimal squeezing angle is dependent upon the interaction time and N [17].

C. Squeezing parameter

For a more quantitative measure of the squeezing, we plot the squeezing parameter (30) for each of the parameters, as shown in Figs. 4(f)–4(j). We observe that for all cases with $U > 0$, at the optimal angle the squeezing parameter is below unity $\chi < 1$, meaning that squeezing is attained on average below the standard quantum limit. A value of $\chi = 1$ corresponds to shot noise at the standard quantum limit, or zero intensity noise in Ref. [67]. Examining the minimum value of χ that is attained, we see that as expected for larger interactions U, generally more squeezing is present, where the best squeezing attained is about $\chi \approx 0.78$ for low-Q cavities [Fig. 4(g)] and $\chi \approx 0.68$ for high-Q cavities [Fig. 4(i)]. We remind the reader that small χ means large squeezing. What is interesting is that for both the low-Q and high-Q cavities, we see that increasing the pump rate A tends to increase squeezing, from $\chi \approx 0.78$ to 0.7 when the pump rate is doubled [Figs. 4(g) and 4(h), respectively]. This again can be explained by the same reason that the Q_N functions show more squeezing for larger N. For larger N, the same squeezing occurs for a shorter time or, put another way, more squeezing is attained for the same time interval. Since larger pumping gives, on average, polaritons that are in larger particle-number sectors N, this results in more squeezing for larger pumping.

We show the effect of the squeezing on the pumping rate A in Fig. 5(a). For each value of A, we choose the optimal spin squeezing angle Φ to show the best squeezing. We see clearly that the squeezing increases monotonically with pumping, for all the parameters chosen. In our simulations, we only consider relatively small polariton numbers due to the limitation of our numerics. Hence, in a realistic experimental situation, the pump rates are likely to be much larger. While we must extrapolate the graphs to larger values, we do not expect that significantly different behavior will occur when the polariton numbers are further increased. The fact that a larger amount of squeezing is obtained for larger pump rates is favorable experimentally, since the realistic polariton numbers are typically much larger than what we consider in our calculations. Hence we expect that the naturally occurring polariton nonlinearities are sufficient to observe squeezing.

We also investigate the effect of the squeezing on the detuning Δ. For exciton-polaritons, in practice, only small detunings would be possible as the pump laser would need to be in resonance with the lower polariton branch. In Fig. 5(b), we see that the detuning does play an important role in enhancing squeezing. The best squeezing occurs when the pump laser

is negatively detuned with respect to the polariton resonance. Qualitatively, we understand this as due to a stabilizing effect of the detuning in the presence of interactions. The effect of the detuning is to apply a phase to the coherent state as seen in (21). At the mean-field level, the interactions U also create a phase on the coherent state. The negative detuning acts to cancel off this interaction-induced phase.

The squeezing as a function of the pumping phase shows a simpler dependence, as shown in Fig. 5(c). We see that the best squeezing occurs when the phases of the pump lasers are matched $\theta_a - \theta_b = n\pi$, where n is an integer. We henceforth set the phases of the pump lasers to $\theta_a - \theta_b = 0$ such as to target the optimally squeezed states. In Fig. 5(d), we see the optimal squeezings in the (A, Δ) plane, the best squeezing is about $\chi \approx 0.60$, corresponding to 2.2 dB squeezing. We see that for larger pumping, the optimal detuning becomes more negative. The amount of squeezing tends to improve with the pumping, as observed before.

V. ENTANGLEMENT DETECTION

The spin squeezing of the exciton-polaritons corresponds to the generation of multiparticle entanglement. In this section, we evaluate two criteria that can be used to detect the entanglement.

A. Wineland squeezing parameter

A simple scheme for detecting entanglement is to use the Wineland squeezing parameter, defined as [74]

$$\xi_N^2 = \frac{N \min_\Phi[\mathrm{Var}_N(S_\Phi)]}{\langle S_x\rangle_N^2 + \langle S_y\rangle_N^2}, \tag{38}$$

where the variance is defined in (28) and the expectation values are taken over a fixed number of particles. In the single particle-number sector N, this is a detector for entanglement if [18]

$$\xi_N^2 < 1. \tag{39}$$

Since in our case the total polariton number is not fixed, (38) would need to be applied for each particle number sector N. In this case it is more appropriate to use the number-fluctuating version of the squeezing parameter defined as [84,85]

$$\xi^2 = \frac{\langle \mathcal{N}\rangle \min_\Phi[\mathrm{Var}(S_\Phi)]}{\langle S_x\rangle^2 + \langle S_y\rangle^2}, \tag{40}$$

where the variance over all particle number sectors is

$$\begin{aligned}\mathrm{Var}(S_\Phi) &= \langle S_\Phi^2\rangle - \langle S_\Phi\rangle^2 \\ &= \mathrm{Tr}(\rho(S_\Phi)^2) - \mathrm{Tr}(\rho(S_\Phi))^2,\end{aligned} \tag{41}$$

and the expectation values are defined over the full ρ, as in (19). All the quantities in (40) can be evaluated in the presence of number fluctuations hence is an experimentally accessible quantity. Entanglement is verified in the system if [84,85]

$$\xi^2 < 1. \tag{42}$$

We show a proof of this in Appendix A. Clearly, in the case of a fixed particle number, state (40) reduces to (38), and the same criterion as (39) is obtained.

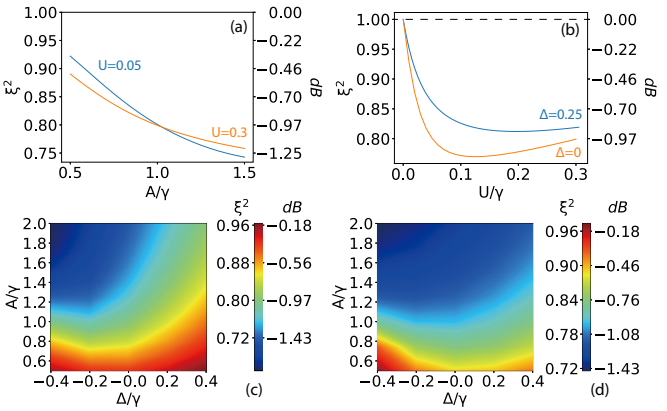

FIG. 6. Wineland squeezing parameter (40) at steady state. Any value of ξ^2 less than 1 indicates entanglement (dashed lines). We plot ξ^2 as a function of (a) pump rate A/γ with $\Delta/\gamma = 0$, $N_{\max} = 20$; (b) interaction strength U/γ with $A/\gamma = 1$, $N_{\max} = 20$; (c) pump rate A/γ and detuning Δ/γ for $U/\gamma = 0.05$, $N_{\max} = 30$; and (d) pump rate A/γ and detuning Δ/γ for $U/\gamma = 0.3$, $N_{\max} = 20$. Common parameters are $V = 0$ and $\theta_a = \theta_b = 0$.

In Figs. 6(a) and 6(b), we show the number-fluctuating Wineland squeezing parameter (40) as a function of the pumping rate A/γ and interaction strength U/γ, respectively. We see that in all cases entanglement can be detected for all parameter choices of A/γ and U/γ. Of particular note is that the squeezing parameter tends to decrease with the pumping rate A/γ [Fig. 6(a)]. Since we expect that the pump rates will be performed at high rates in a realistic experiment, the most relevant regime is for large A/γ. The fact that the squeezing level tends to improve monotonically with A/γ shows that it is favorable to be in the high pumping regime, as also discussed previously. In Fig. 6(b), we see that the squeezing level reaches a minimum with interaction strength and tends to increase thereafter. A similar effect is seen for the detuning, where there is an optimal value. In Figs. 6(c) and 6(d), the squeezing is plotted in the two-dimensional parameter space of A/γ and Δ/γ. Here we see that the squeezing tends to generally improve with A/γ but there is an optimal value of Δ/γ for a given pump rate. This dependence was also seen in Fig. 5(d), where there was an optimal detuning for the best squeezing. Returning to Fig. 6(b), we attribute the optimal value of U/γ for the squeezing to be due to a similar effect to the detuning. Comparing Figs. 6(c) and 6(d), we interestingly see that similar levels of squeezing are obtained for both cases, despite the larger effective interaction in Fig. 6(d). Thus, a larger interaction does not necessarily always lead to more squeezing. To take full advantage of the nonlinearity of value U/γ, the detuning Δ/γ needs to be adjusted to obtain a highly squeezed state.

B. Optimal spin-squeezing criteria

A potentially more sensitive criterion for entanglement was provided in Ref. [38] involving the first and second moments

of the spin operators,

$$N(N+2) \geqslant \langle S_x^2 \rangle_N + \langle S_y^2 \rangle_N + \langle S_z^2 \rangle_N, \tag{43}$$

$$\mathrm{Var}_N(S_x) + \mathrm{Var}_N(S_y) + \mathrm{Var}_N(S_z) \geqslant 2N, \tag{44}$$

$$(N-1)\mathrm{Var}_N(S_k) \geqslant \langle S_i^2 \rangle_N + \langle S_j^2 \rangle_N - 2N, \tag{45}$$

$$(N-1)[\mathrm{Var}_N(S_i) + \mathrm{Var}_N(S_j)] \geqslant \langle S_k^2 \rangle_N + N(N-2), \tag{46}$$

where i, j, k take all the possible permutations of x, y, z. The above inequalities are valid for separable states, hence, to verify entanglement a violation is required, i.e., that the LHS $<$ RHS. These criteria can detect a large range of entangled states such as Fock states. Again, the number-fluctuating version of the criterion is more suitable in our context and some possibilities are given in Eqs. (15)–(18) of Ref. [85]. For the first two inequalities, we can define their corresponding number-fluctuating versions [85]:

$$\mathcal{E}_1 = \langle S_x^2 \rangle + \langle S_y^2 \rangle + \langle S_z^2 \rangle - \langle \mathcal{N}(\mathcal{N}+2) \rangle, \tag{47}$$

$$\mathcal{E}_2 = \mathrm{Var}(S_x) + \mathrm{Var}(S_y) + \mathrm{Var}(S_z) - 2\langle \mathcal{N} \rangle. \tag{48}$$

For separable states,

$$\mathcal{E}_1 \geqslant 0, \tag{49}$$

$$\mathcal{E}_2 \geqslant 0, \tag{50}$$

hence entanglement is detected if these are violated. The number-fluctuating versions in Ref. [85] for the remaining two criteria are not easily used since the inequalities involve expectation values involving factors $(\mathcal{N}-1)^{-1}$, which diverge for $N = 1$.

We therefore derive our own number-fluctuating versions of the criteria, corresponding to (45) and (46). We first define the quantities

$$\mathcal{E}_3 = \langle S_k^2(\mathcal{N}-1) \rangle - \langle S_k \sqrt{\mathcal{N}-1} \rangle^2 - \langle S_i^2 \rangle - \langle S_j^2 \rangle + 2\langle \mathcal{N} \rangle, \tag{51}$$

$$\mathcal{E}_4 = \langle S_i^2(\mathcal{N}-1) \rangle - \langle S_i \sqrt{\mathcal{N}-1} \rangle^2 + \langle S_j^2(\mathcal{N}-1) \rangle - \langle S_j \sqrt{\mathcal{N}-1} \rangle^2 - \langle S_k^2 \rangle - \langle \mathcal{N}(\mathcal{N}-2) \rangle. \tag{52}$$

These criteria have all quantities evaluated over number-fluctuating states. We show in Appendix B that these quantities can be connected to (45) and (46), respectively, and we may deduce that for separable states

$$\mathcal{E}_3 \geqslant 0, \tag{53}$$

$$\mathcal{E}_4 \geqslant 0. \tag{54}$$

Hence a violation of this inequality detects entanglement.

Evaluating the four quantities (47), (48), (51), and (52), we find that $\mathcal{E}_1 = 0$, $\mathcal{E}_2 > 0$, and $\mathcal{E}_4 > 0$ for all parameters. We hence focus upon $\mathcal{E}_3$ for the entanglement detection; our calculated results are shown in Fig. 7. Figure 7(a) shows $\mathcal{E}_3$ as a function of the pump rate, which again shows that the correlations increasingly correspond to that of an entangled state. This is consistent with what was found with the squeezing parameters χ and ξ^2. In Fig. 7(b), we again see

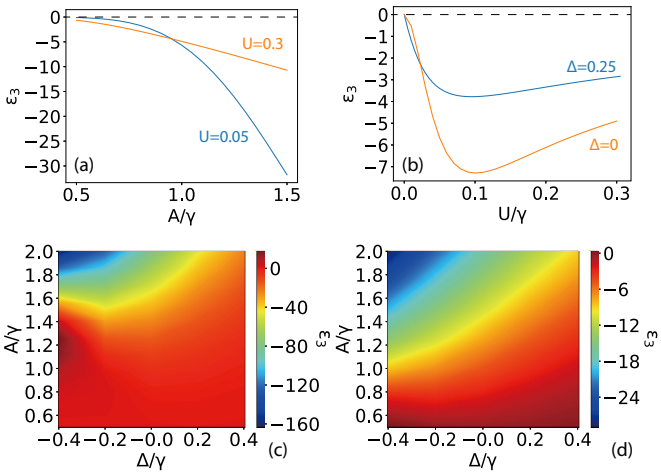

FIG. 7. Spin-squeezing entanglement criterion parameter $\mathcal{E}_3$ from (51) at steady state. In (51), we choose spin directions $i = x$, $j = y$, $k = z$. Any value of $\mathcal{E}_3$ less than 0 indicates entanglement (dashed lines). We plot $\mathcal{E}_3$ as a function of (a) pump rate A/γ with $\Delta/\gamma = 0$, $N_{\max} = 20$; (b) interaction strength U/γ with $A/\gamma = 1$, $N_{\max} = 20$; (c) pump rate A/γ and detuning Δ/γ for $U/\gamma = 0.05$, $N_{\max} = 30$; and (d) pump rate A/γ and detuning Δ/γ for $U/\gamma = 0.3$, $N_{\max} = 20$. Common parameters are $V = 0$ and $\theta_a = \theta_b = 0$.

that the presence of interactions U/γ produces an entangled state, but the level of violation starts to decrease. This is the same behavior as that seen for the Wineland squeezing parameter in Fig. 6(b). The behavior of $\mathcal{E}_3$ as a function of A/γ and Δ/γ is shown in Figs. 7(c) and 7(d). Generally, a very similar behavior with the parameters are seen for both cases $U/\gamma = 0.05, 0.3$. The region of violation for ξ^2 and $\mathcal{E}_3$ is seen to be very similar, with a small region around $\Delta/\gamma < 0$ and $A/\gamma \sim 1$ failing to be detected. With the exception of this small region in parameter space, generally both criteria work very well in detecting entanglement. We thus find that both quantities tend to be quite similar in performance for this particular system. In terms of evaluation, $\mathcal{E}_3$ does not require any optimization (except for the choice of spin axes) and hence may be advantageous in this regard.

VI. SUMMARY AND CONCLUSIONS

We find that it is possible to generate spin-squeezed entanglement at the steady state with exciton-polaritons. The spin squeezing is defined by mapping two spin modes of the exciton-polaritons onto an effective spin space. Using the spin mapping, it is possible to evaluate spin variances, Q functions, and entanglement criteria to show the level of spin squeezing present. The best squeezing is observed for large pump rates A/γ and large self-interactions U/γ. While it is expected that large self-interactions should give an enhanced squeezing, it is fortuitous that large pumping also contributes to better squeezing. This occurs due to the fact that the optimal squeezing time for a S_z^2 interaction scales as $\propto 1/N^{2/3}$. Hence, for highly pumped systems with large average N, only a short interaction time is required. Hence even for low-Q cavities where the time that the polariton spends in the cavity is short, significant squeezing should be able to be generated within this time for large polariton populations. Similar results have

been found in experiments with cold atoms [72]. Interestingly, there is an optimal detuning of the pumping with respect to the squeezing. For larger pumping, the optimal detuning becomes larger. This behavior was observed in polariton experiments where large pump power [67] or detuning [68,86] led to intensity squeezing of light. At higher pump power, detuning requires optimization to find the sweet spot. In an experimental situation, this can be performed by sweeping the frequency of the pump laser.

Squeezing levels can be improved with high-Q cavities as expected. The effect of the high-Q cavities is the increase in magnitude of all the parameters, but considering the relatively limited tunability of U, the largest impact this has is to be able to access effectively larger interaction regions. In this paper, we limited ourselves to naturally occurring values of the polariton-polariton interaction, but numerous studies have examined methods of enhancing it, which would improve squeezing levels. These include using creating dipole interactions between polaritons [87,88] or using charged excitons [89,90]. There are also methods and proposals to achieve polariton blockade in the weak interaction regime [53,91–93]. To take advantage of the larger nonlinearities, it is required to tune the detuning parameter to generate the largest squeezing levels. Our results show that even for a small nonlinearity, this can effectively be compensated by applying a large pump rate at the appropriate detuning. While in our ideal theoretical calculations this may be true, we expect that in practice other sources of decoherence may be present, where it would be advantageous to have high-Q cavities. In our calculations, the main source of decoherence—loss—is included but other types of decoherence which may be detrimental to working at the standard quantum limit may also be present. Hence, while our results are promising to observe entanglement in polariton condensates, further studies should include other sources of decoherence. We also note that there should also be squeezing present in the transient dynamics (e.g., $t = 0$ to $t = 1/\gamma$) before going to the steady state. While it might be possible to see even stronger squeezing by looking at the transient dynamics, this will probably add more complex experimental challenges as Q functions and spin measurements must be measured on the picosecond timescale. Hence, in the interest of simplicity of the experimental demands we did not examine this, although this may also be an interesting avenue of future research.

ACKNOWLEDGMENTS

This work is supported by the Shanghai Research Challenge Fund; New York University Global Seed Grants for Collaborative Research, National Natural Science Foundation of China (61571301), the Thousand Talents Program for Distinguished Young Scholars (D1210036A), and the NSFC Research Fund for International Young Scientists (11650110425), NYU-ECNU Institute of Physics at NYU Shanghai, the Science and Technology Commission of Shanghai Municipality (17ZR1443600), the China Science and Technology Exchange Center (NGA-16-001), and A.N.P. acknowledges support from the State assignment (AAAA-A19-119071190017-7).

APPENDIX A: PROOF OF NUMBER FLUCTUATING WINELAND SQUEEZING CRITERION

Following Ref. [18], we first consider a number fluctuating separable state of the form

$$\rho = \sum_{k,N} P_{kN} \rho_{kN}^{(1)} \otimes \cdots \otimes \rho_{kN}^{(N)}. \tag{A1}$$

Here the density matrices for the ith particle is denoted $\rho_{kN}^{(i)}$, and the probability of obtaining the kth spin ensemble containing N particles is P_{kN}, where

$$\sum_{k,N} P_{kN} = 1. \tag{A2}$$

In this notation, the total spin operators are defined as

$$S_j = \sum_i \sigma_j^{(i)}, \tag{A3}$$

where $j \in \{x, y, z\}$ and i labels the particles. Spin expectations can be calculated as

$$\langle S_z \rangle = \sum_{k,N} P_{kN} \sum_i \langle \sigma_z^{(i)} \rangle_{kN}, \tag{A4}$$

where the expectation value over subspins is defined as

$$\langle \sigma_z^{(i)} \rangle_{kN} = \mathrm{Tr}\big(\sigma_z^{(i)} \rho_{kN}^{(i)}\big). \tag{A5}$$

We can then evaluate that

$$\begin{aligned} \mathrm{Var}(S_z) &= \langle S_z^2 \rangle - \langle S_z \rangle^2 \\ &= \langle \mathcal{N} \rangle - \sum_{k,N} P_{kN} \sum_i \langle \sigma_z^{(i)} \rangle_{kN}^2 \\ &\quad + \sum_{k,N} P_{kN} \langle S_z \rangle_{kN}^2 - \langle S_z \rangle^2, \end{aligned} \tag{A6}$$

where we defined the average particle number:

$$\langle \mathcal{N} \rangle = \sum_{k,N} P_{kN} N. \tag{A7}$$

We now find the three inequalities as in Ref. [18]. First, using the Cauchy-Schwartz inequality, we have

$$\begin{aligned} \langle S_z \rangle^2 &= \left(\sum_{k,N} P_{kN} \langle S_z \rangle_{kN} \right)^2 \\ &\leqslant \sum_{k,N} P_{kN} \langle S_z \rangle_{kN}^2. \end{aligned} \tag{A8}$$

Second, starting from

$$\langle \sigma_x^{(i)} \rangle_{kN}^2 + \langle \sigma_y^{(i)} \rangle_{kN}^2 + \langle \sigma_z^{(i)} \rangle_{kN}^2 \leqslant 1, \tag{A9}$$

we multiply by P_{kN} and sum over k, N, i to obtain

$$\begin{aligned} -\sum_{k,N} P_{kN} \sum_i \langle \sigma_z^{(i)} \rangle_{kN}^2 \geqslant &- \langle \mathcal{N} \rangle + \sum_{k,N} P_{kN} \sum_i \langle \sigma_x^{(i)} \rangle_{kN}^2 \\ &+ \sum_{k,N} P_{kN} \sum_i \langle \sigma_y^{(i)} \rangle_{kN}^2. \end{aligned} \tag{A10}$$

Finally, again using the Cauchy-Schwartz inequality, we have

$$\langle S_x\rangle^2 = \left(\sum_{k,N,i} P_{kN}\langle\sigma_x^{(i)}\rangle_{kN}\right)^2 \leqslant \langle\mathcal{N}\rangle \sum_{k,N} P_{kN} \sum_i \langle\sigma_x^{(i)}\rangle_{kN}^2. \tag{A11}$$

Finding the same inequality for $\langle S_y\rangle^2$ and adding, we thus have

$$\langle S_x\rangle^2+\langle S_y\rangle^2 \leqslant \langle\mathcal{N}\rangle \sum_{k,N} P_{kN} \sum_i \left(\langle\sigma_x^{(i)}\rangle_{kN}^2 + \langle\sigma_y^{(i)}\rangle_{kN}^2\right). \tag{A12}$$

Substituting (A6), (A8), (A10), and (A12) into (40) to obtain an upper bound, we obtain the criterion (42).

APPENDIX B: PROOF OF NUMBER FLUCTUATING OPTIMAL SPIN INEQUALITY

In this Appendix, we show that for separable states (53) and (54) hold.

1. Proof of Eq. (53)

First consider the second term in (51). Due to the number-conserving nature of the operator $S_k\sqrt{\mathcal{N}-1}$, we can use a similar argument to (19) to write

$$\begin{aligned}\langle S_k\sqrt{\mathcal{N}-1}\rangle^2 &= \left(\sum_N p_N\langle S_k\sqrt{\mathcal{N}-1}\rangle_N\right)^2 \\ &\leqslant \sum_N p_N\langle S_k\sqrt{\mathcal{N}-1}\rangle_N^2 \\ &= \sum_N p_N(N-1)\langle S_k\rangle_N^2,\end{aligned} \tag{B1}$$

where in the second line we used the Cauchy-Schwartz relation $E(XY)^2 \leqslant E(X^2)E(Y^2)$ where $Y=1$ in this case. Meanwhile, all the other terms can be directly written as a sum over N using similar arguments to (19). For example, the first term in (51) is

$$\langle(\mathcal{N}-1)S_k^2\rangle = \sum_N p_N(N-1)\langle S_k^2\rangle_N. \tag{B2}$$

Putting these expressions into (51), we obtain

$$\begin{aligned}\mathcal{E}_3 \geqslant \sum_N p_N\big[&(N-1)\langle S_k^2\rangle_N - (N-1)\langle S_k\rangle_N^2 \\ &- \langle S_i^2\rangle_N - \langle S_j^2\rangle_N + 2N\big].\end{aligned} \tag{B3}$$

The quantity in the square brackets is exactly (45), hence we conclude that $\mathcal{E}_3 \geqslant 0$ for any separable state.

2. Proof of Eq. (54)

Using (B1), (B2), and similar arguments in (19), we can write

$$\begin{aligned}\mathcal{E}_4 \geqslant \sum_N p_N\big[&(N-1)\langle S_i^2\rangle_N - (N-1)\langle S_i\rangle_N^2 + (N-1)\langle S_j^2\rangle_N \\ &- (N-1)\langle S_j\rangle_N^2 - \langle S_k^2\rangle_N - N(N-2)\big]\end{aligned}$$

The quantity in the square brackets is exactly (46), hence we conclude that $\mathcal{E}_4 \geqslant 0$ for any separable state.

[1] R. Horodecki, P. Horodecki, M. Horodecki, and K. Horodecki, Rev. Mod. Phys. **81**, 865 (2009).
[2] W. K. Wootters and W. S. Leng, Philos. Trans.: Math. Phys. Eng. Sci. **356**, 1717 (1998).
[3] J. Bub, *Quantum Entanglement and Information*, Summer 2020 ed. (Metaphysics Research Lab, Stanford University, Redwood City, California, 2020).
[4] K. Życzkowski, P. Horodecki, M. Horodecki, and R. Horodecki, Phys. Rev. A **65**, 012101 (2001).
[5] V. Vedral, M. B. Plenio, M. A. Rippin, and P. L. Knight, Phys. Rev. Lett. **78**, 2275 (1997).
[6] B. Julsgaard, A. Kozhekin, and E. S. Polzik, Nature **413**, 400 (2001).
[7] H. Krauter, D. Salart, C. A. Muschik, J. M. Petersen, H. Shen, T. Fernholz, and E. S. Polzik, Nat. Phys. **9**, 400 (2013).
[8] H. Krauter, C. A. Muschik, K. Jensen, W. Wasilewski, J. M. Petersen, J. I. Cirac, and E. S. Polzik, Phys. Rev. Lett. **107**, 080503 (2011).
[9] L. Pezzè, A. Smerzi, M. K. Oberthaler, R. Schmied, and P. Treutlein, Rev. Mod. Phys. **90**, 035005 (2018).
[10] D. R. Nelson, Phys. Rev. Lett. **60**, 1973 (1988).
[11] L. DiCarlo, M. D. Reed, L. Sun, B. R. Johnson, J. M. Chow, J. M. Gambetta, L. Frunzio, S. M. Girvin, M. H. Devoret, and R. J. Schoelkopf, Nature **467**, 574-578 (2010).
[12] A. Berkley, H. Xu, R. Ramos, M. Gubrud, F. Strauch, P. Johnson, J. Anderson, A. Dragt, C. Lobb, and F. Wellstood, Science **300**, 1548 (2003).
[13] G. B. Lesovik, T. Martin, and G. Blatter, Eur. Phys. J. Phys. B **24**, 287 (2001).
[14] M. Kitagawa and M. Ueda, Phys. Rev. A **47**, 5138 (1993).
[15] M. M. Nieto and D. R. Truax, Phys. Rev. Lett. **71**, 2843 (1993).
[16] R. E. Slusher, L. W. Hollberg, B. Yurke, J. C. Mertz, and J. F. Valley, Phys. Rev. Lett. **55**, 2409 (1985).
[17] T. Byrnes and E. O. Ilo-Okeke, *Quantum Atom Optics: Theory and Applications to Quantum Technology* (Cambridge University Press, Cambridge, 2021).
[18] A. Sørensen, L.-M. Duan, J. I. Cirac, and P. Zoller, Nature **409**, 63 (2001).
[19] C. Gross, J. Phys. B: At., Mol. Opt. Phys. **45**, 103001 (2012).
[20] C. Gross, J. Esteve, A. Weller, S. Giovanazzi, E. Nicklas, T. Zibold, and M. Oberthaler, *Laser Spectroscopy* (World Scientific, Singapore, 2010), pp. 19–28.
[21] A. S. Sørensen and K. Mølmer, Phys. Rev. Lett. **86**, 4431 (2001).

[22] H. Strobel, W. Muessel, D. Linnemann, T. Zibold, D. B. Hume, L. Pezzè, A. Smerzi, and M. K. Oberthaler, Science **345**, 424 (2014).

[23] M. Fadel, T. Zibold, B. Décamps, and P. Treutlein, Science **360**, 409 (2018).

[24] P. Kunkel, M. Prüfer, H. Strobel, D. Linnemann, A. Frölian, T. Gasenzer, M. Gärttner, and M. K. Oberthaler, Science **360**, 413 (2018).

[25] K. Lange, J. Peise, B. Lücke, I. Kruse, G. Vitagliano, I. Apellaniz, M. Kleinmann, G. Tóth, and C. Klempt, Science **360**, 416 (2018).

[26] Z.-H. Ma, J. Cui, Z. Cao, S.-M. Fei, V. Vedral, T. Byrnes, and C. Radhakrishnan, Europhys. Lett. **125**, 50005 (2019).

[27] P. Treutlein, T. W. Hänsch, J. Reichel, A. Negretti, M. A. Cirone, and T. Calarco, Phys. Rev. A **74**, 022312 (2006).

[28] Y. Jing, M. Fadel, V. Ivannikov, and T. Byrnes, New J. Phys. **21**, 093038 (2019).

[29] J. Kitzinger, M. Chaudhary, M. Kondappan, V. Ivannikov, and T. Byrnes, Phys. Rev. Research **2**, 033504 (2020).

[30] S. Idlas, L. Domenzain, R. Spreeuw, and T. Byrnes, Phys. Rev. A **93**, 022319 (2016).

[31] A. N. Pyrkov and T. Byrnes, New J. Phys. **15**, 093019 (2013).

[32] O. Pettersson and T. Byrnes, Phys. Rev. A **95**, 043817 (2017).

[33] E. O. Ilo-Okeke and T. Byrnes, Phys. Rev. Lett. **112**, 233602 (2014).

[34] D. Rosseau, Q. Ha, and T. Byrnes, Phys. Rev. A **90**, 052315 (2014).

[35] M. I. Hussain, E. O. Ilo-Okeke, and T. Byrnes, Phys. Rev. A **89**, 053607 (2014).

[36] T. Byrnes, K. Wen, and Y. Yamamoto, Phys. Rev. A **85**, 040306(R) (2012).

[37] A. Abdelrahman, T. Mukai, H. Häffner, and T. Byrnes, Optics Express **22**, 3501 (2014).

[38] G. Tóth, C. Knapp, O. Gühne, and H. J. Briegel, Phys. Rev. A **79**, 042334 (2009).

[39] M. F. Riedel, P. Böhi, Y. Li, T. W. Hänsch, A. Sinatra, and P. Treutlein, Nature **464**, 1170 (2010).

[40] J. Kasprzak, M. Richard, S. Kundermann, A. Baas, P. Jeambrun, J. M. J. Keeling, F. M. Marchetti, M. H. Szymańska, R. André, J. L. Staehli *et al.*, Nature **443**, 409 (2006).

[41] H. Deng, H. Haug, and Y. Yamamoto, Rev. Mod. Phys. **82**, 1489 (2010).

[42] A. Kavokin, Phys. Status Solidi B **247**, 1898 (2010).

[43] M. Richard, J. Kasprzak, A. Baas, K. Lagoudakis, M. Wouters, I. Carusotto, R. André, B. Deveaud, S. Le, and D. le si, Int. J. Nanotechnology **7**, 668 (2010).

[44] D. Snoke and P. Littlewood, Phys. Today **63**, 42 (2010).

[45] J. Keeling and N. G. Berloff, Contemp. Phys. **52**, 131 (2011).

[46] *Exciton Polaritons in Microcavities*, edited by V. Timofeev and D. Sanvitto (Springer, Berlin, 2012).

[47] I. Carusotto and C. Ciuti, Rev. Mod. Phys. **85**, 299 (2013).

[48] T. Byrnes, N. Y. Kim, and Y. Yamamoto, Nat. Phys. **10**, 803 (2014).

[49] R. Balili, V. Hartwell, D. Snoke, L. Pfeiffer, and K. West, Science (New York, N.Y.) **316**, 1007 (2007).

[50] H. Deng, G. Weihs, C. Santori, J. Bloch, and Y. Yamamoto, Science **298**, 199 (2002).

[51] C. Ciuti, V. Savona, C. Piermarocchi, A. Quattropani, and P. Schwendimann, Phys. Rev. B **58**, 7926 (1998).

[52] T. Byrnes, P. Recher, and Y. Yamamoto, Phys. Rev. B **81**, 205312 (2010).

[53] T. Byrnes, G. V. Kolmakov, R. Y. Kezerashvili, and Y. Yamamoto, Phys. Rev. B **90**, 125314 (2014).

[54] T. Horikiri, M. Yamaguchi, K. Kamide, Y. Matsuo, T. Byrnes, N. Ishida, A. Löffler, S. Höfling, Y. Shikano, T. Ogawa, A. Forchel, and Y. Yamamoto, Sci. Rep. **6**, 25655 (2016).

[55] A. Amo, T. Liew, C. Adrados, R. Houdré, E. Giacobino, A. Kavokin, and A. Bramati, Nat. Photonics **4**, 361 (2010).

[56] F. I. Moxley III, J. P. Dowling, W. Dai, and T. Byrnes, Phys. Rev. A **93**, 053603 (2016).

[57] D. Ballarini, M. De Giorgi, E. Cancellieri, R. Houdré, E. Giacobino, R. Cingolani, A. Bramati, G. Gigli, and D. Sanvitto, Nat. Commun. **4**, 1778 (2013).

[58] N. Ishida, T. Byrnes, F. Nori, and Y. Yamamoto, Sci. Rep. **3**, 1180 (2013).

[59] A. Amo, S. Pigeon, D. Sanvitto, V. Sala, R. Hivet, I. Carusotto, F. Pisanello, G. Leménager, R. Houdré, E. Giacobino *et al.*, Science **332**, 1167 (2011).

[60] N. Masumoto, N. Y. Kim, T. Byrnes, K. Kusudo, A. Löffler, S. Höfling, A. Forchel, and Y. Yamamoto, New J. Phys. **14**, 065002 (2012).

[61] C. Schneider, A. Rahimi-Iman, N. Y. Kim, J. Fischer, I. G. Savenko, M. Amthor, M. Lermer, A. Wolf, L. Worschech, V. D. Kulakovskii *et al.*, Nature **497**, 348 (2013).

[62] S. Christopoulos, G. Baldassarri Hoger von Högersthal, A. Grundy, P. G. Lagoudakis, A. V. Kavokin, J. J. Baumberg, G. Christmann, R. Butté, E. Feltin, J.-F. Carlin, and N. Grandjean, Phys. Rev. Lett. **98**, 126405 (2007).

[63] J. J. Baumberg, A. V. Kavokin, S. Christopoulos, A. J. D. Grundy, R. Butté, G. Christmann, D. D. Solnyshkov, G. Malpuech, G. Baldassarri Höger von Högersthal, E. Feltin *et al.*, Phys. Rev. Lett. **101**, 136409 (2008).

[64] S. Kéna-Cohen and S. R. Forrest, Nat. Photonics **4**, 371 (2010).

[65] T. Guillet, M. Mexis, J. Levrat, G. Rossbach, C. Brimont, T. Bretagnon, B. Gil, R. Butté, N. Grandjean, L. Orosz *et al.*, Appl. Phys. Lett. **99**, 161104 (2011).

[66] J. D. Plumhof, T. Stöferle, L. Mai, U. Scherf, and R. F. Mahrt, Nat. Mater. **13**, 247 (2014).

[67] T. Boulier, M. Bamba, A. Amo, C. Adrados, A. Lemaitre, E. Galopin, I. Sagnes, J. Bloch, C. Ciuti, E. Giacobino *et al.*, Nat. Commun. **5**, 3260 (2014).

[68] J. P. Karr, A. Baas, R. Houdré, and E. Giacobino, Phys. Rev. A **69**, 031802(R) (2004).

[69] A. F. Adiyatullin, M. D. Anderson, H. Flayac, M. T. Portella-Oberli, F. Jabeen, C. Ouellet-Plamondon, G. C. Sallen, and B. Deveaud, Nat. Commun. **8**, 1329 (2017).

[70] Á. Cuevas, J. C. L. Carreño, B. Silva, M. De Giorgi, D. G. Suárez-Forero, C. S. Muñoz, A. Fieramosca, F. Cardano, L. Marrucci, V. Tasco *et al.*, Sci. Adv. **4**, eaao6814 (2018).

[71] S. M. Tan, Phys. Rev. A **60**, 2752 (1999).

[72] V. Josse, A. Dantan, L. Vernac, A. Bramati, M. Pinard, and E. Giacobino, Phys. Rev. Lett. **91**, 103601 (2003).

[73] V. Josse, A. Dantan, A. Bramati, M. Pinard, and E. Giacobino, Phys. Rev. Lett. **92**, 123601 (2004).

[74] D. J. Wineland, J. J. Bollinger, W. M. Itano, and D. J. Heinzen, Phys. Rev. A **50**, 67 (1994).

[75] C. T. Lee, Phys. Rev. A **30**, 3308 (1984).
[76] C. Joana, P. van Loock, H. Deng, and T. Byrnes, Phys. Rev. A **94**, 063802 (2016).
[77] T. C. H. Liew, A. V. Kavokin, and I. A. Shelykh, Phys. Rev. Lett. **101**, 016402 (2008).
[78] S. I. Tsintzos, A. Tzimis, G. Stavrinidis, A. Trifonov, Z. Hatzopoulos, J. J. Baumberg, H. Ohadi, and P. G. Savvidis, Phys. Rev. Lett. **121**, 037401 (2018).
[79] N. Takemura, S. Trebaol, M. Wouters, M. T. Portella-Oberli, and B. Deveaud, Nat. Phys. **10**, 500 (2014).
[80] N. Takemura, M. D. Anderson, M. Navadeh-Toupchi, D. Y. Oberli, M. T. Portella-Oberli, and B. Deveaud, Phys. Rev. B **95**, 205303 (2017).
[81] M. Wouters, Phys. Rev. B **76**, 045319 (2007).
[82] J. Johansson, P. Nation, and F. Nori, Comput. Phys. Commun. **184**, 1234 (2013).
[83] J. Johansson, P. Nation, and F. Nori, Comput. Phys. Commun. **183**, 1760 (2012).
[84] P. Hyllus, L. Pezzé, and A. Smerzi, Phys. Rev. Lett. **105**, 120501 (2010).
[85] P. Hyllus, L. Pezzé, A. Smerzi, and G. Tóth, Phys. Rev. A **86**, 012337 (2012).
[86] M. Romanelli, J. P. Karr, C. Leyder, E. Giacobino, and A. Bramati, Phys. Rev. B **82**, 155313 (2010).
[87] I. Rosenberg, D. Liran, Y. Mazuz-Harpaz, K. West, L. Pfeiffer, and R. Rapaport, Sci. Adv. **4**, eaat8880 (2018).
[88] E. Togan, H.-T. Lim, S. Faelt, W. Wegscheider, and A. Imamoglu, Phys. Rev. Lett. **121**, 227402 (2018).
[89] R. P. A. Emmanuele, M. Sich, O. Kyriienko, V. Shahnazaryan, F. Withers, A. Catanzaro, P. M. Walker, F. A. Benimetskiy, M. S. Skolnick, A. I. Tartakovskii *et al.*, Nat. Commun. **11**, 3589 (2020).
[90] M. Sidler, P. Back, O. Cotlet, A. Srivastava, T. Fink, M. Kroner, E. Demler, and A. Imamoglu, Nat. Phys. **13**, 255 (2017).
[91] O. Kyriienko and T. C. H. Liew, Phys. Rev. B **93**, 035301 (2016).
[92] S. V. Andreev, Phys. Rev. B **101**, 125129 (2020).
[93] M.-A. Lemonde, N. Didier, and A. A. Clerk, Phys. Rev. A **90**, 063824 (2014).